Effect of Supercritical Carbon Dioxide Processing on Ionic Association and Conduction in a Crystalline Poly(ethylene oxide)−$LiCF_3SO_3$ Complex

Yoichi Tominaga, Yasuyuki Izumi, Gun-Ho Kwak, Shigeo Asai, and Masao Sumita*

Department of Chemistry and Materials Science, Tokyo Institute of Technology, Ookayama, Tokyo 152-8552, Japan

Received April 7, 2003; Revised Manuscript Received July 21, 2003

ABSTRACT: To achieve fast ion transport in poly(ethylene oxide) (PEO)-based polymer electrolytes, we aimed to increase the ionic conductivity by using supercritical carbon dioxide ($scCO_2$) as a processing solvent. In the crystalline PEO−$LiCF_3SO_3$ complex system, a large difference was observed in the conductivities of the original and $scCO_2$-treated samples. In particular, PEO_7–$LiCF_3SO_3$ (oxyethylene unit:Li = 7:1) increased in conductivity approximately 100-fold at 40 °C with $scCO_2$ processing to a value of 1.8×10^{-5} S/cm. Differential scanning calorimetry measurement showed that the processing reduces the glass transition temperature (T_g), the melting point of the PEO crystalline phase (T_{m1}), and the heat of fusion of the crystalline complex part (ΔH_2). Raman scattering analysis clearly confirmed the decrease in the triple ion fraction and the increase in the ion pair fraction in $scCO_2$-treated samples. Furthermore, subsequent time dependence of the ionic conductivity shows that $scCO_2$ processing maintains the conductivity more than 10-fold higher for at least one month. As a mechanism, we believe that the CO_2 molecules permeated into the sample play a crucial role in the dissociation of ions to increase the conductivity, according to the Lewis acid−base interaction.

Introduction

Ion-conductive polymer electrolytes such as poly(ethylene oxide) (PEO)−metal salt complexes[1] are winning interest as solid-state alternatives to liquid electrolytes for electrochemical device applications. These range from batteries[2,3] to solar cells,[4] fuel cells,[5,6] and electrochromic displays.[7] Above all, secondary lithium batteries based on polymer electrolytes have the capability of outstanding performance in terms of mechanical stability, reliability, and safety. There have recently been many studies on the macromolecular design of PEO-based polymers as electrolyte materials with mainly reduced degrees of crystallinity, showing good electrochemical stability, and improvement in salt solubility.[7−9] However, these materials suffer from a relatively low ionic conductivity in the solid state compared with most liquid or ceramic electrolytes. Fast migration of ions in a polymer can be realized by increasing the local chain mobility, since ions are transported via the segmental motion of ether chains. The localized structure that plays a crucial role for the ionic conduction is believed to involve cation−anion or cation−dipole interactions.[10] Unfortunately, the ionic interaction sometimes inhibits conduction of ions because of their strong cohesion, which increases the glass transition temperature (T_g). For fast migration of ions, a technique that can modify the localized polar structure containing ions is needed. In our previous work we reported improvements in ionic conductivity for simple polyether−salt mixtures processed in CO_2 under supercritical conditions.[11,12] In an amorphous poly(oligooxyethylene methacrylate)−$LiCF_3SO_3$ complex, we found a large increase in the room temperature conductivity on using CO_2 as processing solvent.[12]

Supercritical carbon dioxide ($scCO_2$) has recently attracted much interest as a solvent for polymer processing and synthesis as a result of its extraordinary properties.[13,14] It is also convenient because of its accessible critical point (T_c = 31.1 °C, P_c = 7.4 MPa), its nontoxicity, and its nonflammability. It has high diffusivity and low viscosity like a gas, yet like a liquid it can dissolve a wide range of compounds and small molecules. By controlling the pressure, extremely wide variations in the solvent properties can therefore be achieved. Certainly CO_2 is a good solvent for many nonpolar (and some polar) molecules with low molecular weight,[15] though it is a very poor solvent for most high molecular weight polymers (other than silicones and fluoropolymers[16,17]) under readily achievable conditions. Although the solubility of most polymers in CO_2 is low, the solubility of CO_2 in many polymers is substantial.[18,19] This can lead to a dramatic decrease in T_g, i.e., plasticization, even at modest pressures. For example, the T_g of syndiotactic polystyrene was reduced by up to 30 °C under a CO_2 pressure of only 35 atm.[20] Several groups have reported that CO_2 is a good plasticizing agent for polymeric materials, including poly(ethylene telephthalate), poly(vinyl chloride), polyethylene, polypropylene, nylon, polyimides, polyurethanes, and polymethacrylates.[18−23] Plasticizing effects are involved in most applications of polymer processing, including the formation of blends, microcellular plastics, and particulate polymers.[14] Under pressurized conditions, CO_2 molecules can easily permeate into polymers, especially amorphous polymers. Kazarian et al. have shown that some polymers possessing electron-donating groups such as carbonyls have specific interactions with CO_2, probably of Lewis acid−base nature.[24,25]

* To whom correspondence should be addressed. Phone: +81-3-5734-2431. Fax: +81-3-5734-2876. E-mail: msumita@o.cc.titech.ac.jp.

10.1021/ma030207n CCC: $25.00
Published on Web 10/02/2003

In our present work, $scCO_2$ is used as the processing solvent for a crystalline PEO−$LiCF_3SO_3$ complex to improve the ionic conductivity. Two effects of the CO_2 processing are expected. One is plasticization of amorphous domains where ionic conduction occurs. The CO_2 molecules can permeate into the sample, and probably modify the localized structure containing ions through the Lewis acid−base interactions. Polyether derivatives are "CO_2-philic" materials, since low molecular weight poly(glycol)s such as poly(propylene oxide) and PEO can dissolve in subcritical and supercritical CO_2.[26] Also, crystalline PEO and complex domains may be reduced with increasing concentration of dissolved CO_2 for processing above the melting point. The second effect of CO_2 processing is expected to be dissociation of ionic species such as the aggregator and crystalline complex, which is largely responsible for increases in T_g. Alkali-metal salts possessing fluorine atoms show relatively high ionic conductivity in liquid CO_2 and $scCO_2$.[27] This shows that the interaction between the quadrupole moment of CO_2 and dipoles such as the CF_3 group makes the salt more CO_2-philic,[28] increasing the solubility.

In this paper, we characterize the changes of ionic association in $scCO_2$-treated PEO−$LiCF_3SO_3$ complexes using Raman spectroscopy. Differential scanning calorimetry (DSC) measurement was also carried out on the samples. We also investigated the stability of the effect of $scCO_2$ processing on ionic conductivity. Our study of the difference in ionic conductivity between the original and the $scCO_2$-treated samples is thoroughly data driven.

Experimental Section

Sample Preparation. PEO (average M_w 500000, Wako Chemical Co.) and lithium trifluoromethanesulfonate ($LiCF_3SO_3$; 96%, Aldrich Co.) were dissolved in excess acetone (special grade, Kanto Chemical Co.) and were mixed at room temperature for 24 h. The composition of a PEO−$LiCF_3SO_3$ system is specified as OE:Li (x), which gives the ratio of the number of oxyethylene units to the number of cations. After mixing, the intermediate gel-like solution was slowly dried in air at 80 °C, and then dried in vacuo at 80 °C for 24 h. The resulting solid products, denoted $PEO_xLiCF_3SO_3$ (Px), were compression-molded into an approximately 1.0 mm thick film at 80 °C (x = 40, 20, 10, and 7) and at 180 °C (x = 5 and 3) for 10 min under a pressure of 20 MPa, and then dried in vacuo at room temperature for 24 h.

The $scCO_2$ treatment samples were prepared using a $scCO_2$ extraction system (JASCO Co., Ltd.) consisting of a delivery pump (SCF-Get), an automatic back-pressure regulator (SCF-Bpg), and a heater. A high-pressure reactor (max 35 MPa, 400 °C) made of SUS−Ni alloy (Hastelloy) was constructed from a retainer and a vessel (80 mL) with a Au-coated copper seal. Liquid CO_2 was pumped into the reactor from the delivery pump at a rate of 2.0 mL/min. The sample films were treated with $scCO_2$ in the reactor at 100 °C, which is higher than the melting point of PEO, at 20 MPa for 30 min. The reactor was cooled to 20 °C in cold water while the pressure was held constant. Immediately after cooling, the extra CO_2 gas was released. The films were dried in vacuo at 30 °C for 24 h. The appearance of these sample films varied from transparent to slightly opaque.

Measurements. The ionic conductivity of all the samples was measured by a complex ac impedance method using a 4192A LF impedance analyzer (Hewlett-Packard) in the frequency range 100 Hz−13 MHz. The temperature was increased from 30 to 100 °C at a heating rate of 2.0 °C/min using a temperature controller (KP-1000, CHINO Co.). The sample was sandwiched between two SUS electrodes with a 1.0 mm thick Teflon spacer, and the cell surface was then insulated using polyimide tape. The entire process was carried out in an SUS box filled with dry N_2 gas. The resulting time dependence of the ionic conductivity was measured using P7 samples which were preserved under dry N_2 gas for 30 days.

The DSC measurement was carried out using a Shimadzu Co. system consisting of a DSC-50 and TA-50WS. The temperature was increased from −100 to +200 °C at a heating rate of 10 °C/min.

The Raman scattering spectra at room temperature were recorded on a JASCO FT-IR spectrometer system (FT-IR 800) built into a Raman laser unit (RFT-800) in the region 1200−400 cm^{-1} with a resolution of 2.0 cm^{-1}. The 1064 nm line of a Nd:YAG laser operating at 0.8 mW was used as excitation. The resulting bands were curve-fitted by a nonlinear least-squares method with an original curve resolution program using a straight baseline and a Gaussian product function for each band.

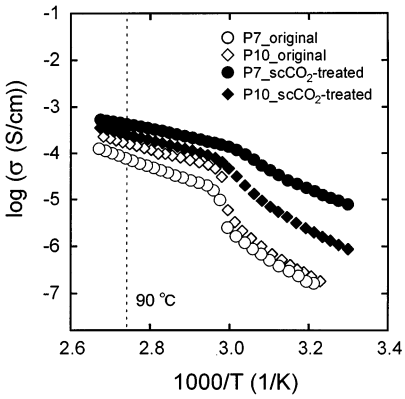

Figure 1. Temperature dependence of ionic conductivity for the original and $scCO_2$-treated samples of P10 and P7.

Results and Discussion

Ac Impedance Measurement. Figure 1 shows the temperature dependence of the ionic conductivity for original and $scCO_2$-treated samples of both P10 and P7. The two original samples had a low conductivity, on the order of 10^{-7} S/cm at room temperature, because of a transition at approximately 60 °C corresponding to the melting temperature of crystalline PEO domains. Above the transition point, the conductivity increases linearly with temperature and the temperature dependence essentially follows an Arrhenius-type equation. In this region, the conductivity of the P7 sample is slightly lower than that of P10, since the glass transition temperature (T_g) increases with increasing salt concentration. Conductivity is related to the PEO chain mobility of the local structure, on the basis of the ion−dipole interactions between the cation and ether oxygen which have a considerable influence on ionic conduction. These data are in accord with the results on Robitaille and Fauteux.[29] On the other hand, the conductivity of $scCO_2$-treated samples was higher than that of the original over the entire temperature range measured. In particular, the conductivity of the P7 sample at lower temperatures was more than 100-fold greater (it was 1.8×10^{-5} S/cm at 40 °C), and that of P10 was approximately 10-fold greater at room temperature. Simultaneously, decreases in the transition temperature around 60 °C, corresponding to the melting of the crystal PEO part, were also observed. The slope of the Arrhenius plots, showing the apparent activation energy, was also lowered by $scCO_2$ processing. In the high-temperature range, the conductivity of $scCO_2$-treated samples remained high. Complex impedance curves at 90 °C, plotting Z_{real} vs Z_{imag}, are shown in Figure 2. The bulk

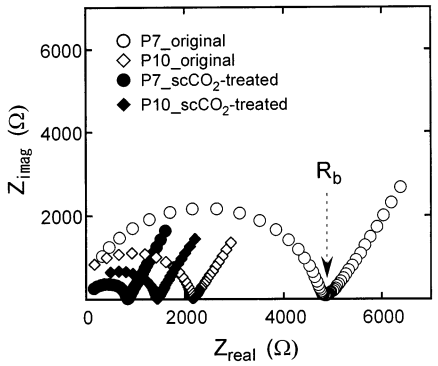

Figure 2. Cole−Cole plots of the samples in Figure 1 at 90 °C.

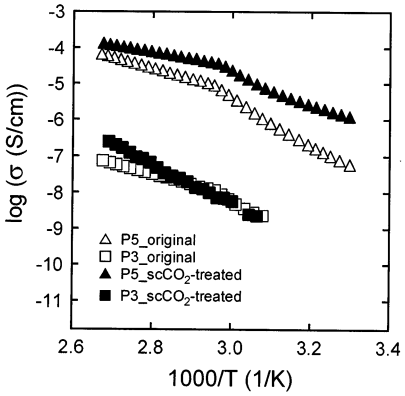

Figure 3. Temperature dependence of ionic conductivity for the original and $scCO_2$-treated samples of P5 and P3.

resistance of each sample, R_b, is estimated from the intersection of the curve and the *x*-axis. Ionic conductivity can be calculated from R_b using the equation $\sigma_i = d/(AR_b)$, where *d* is the sample thickness and *A* is the area. Figure 2 clearly shows reduction in R_b for each $scCO_2$-treated sample; in particular the P7 sample was less than 1 kΩ, whereas R_b for the original sample was approximately 5 kΩ. The $scCO_2$-treated sample of P7 had a lower R_b than P10, whereas the R_b of the P7 original sample is higher than that of P10.

Figure 3 also shows the temperature dependence of the ionic conductivity for the P5 and P3 samples. The conductivity of the P5 sample was also increased by the $scCO_2$ processing, by up to approximately 10-fold at room temperature. Apparent reductions of the transition discontinuity for $scCO_2$-treated samples corresponding to the PEO crystal are seen in these plots, as in the P10 and P7 samples. However, the sample with the highest salt concentration, P3, showed extremely low conductivity. Bruce et al. found that the PEO forms a highly crystalline complex with $LiCF_3SO_3$, on the basis of the stereochemical structure which was characterized in detail by powder X-ray diffraction data.[30] According to this report, it is impossible for ions to migrate in the crystalline complex domains, because Li cations are strongly coordinated by five oxygens. These comprise three ether oxygens and one oxygen from each of two adjacent CF_3SO_3 anions. Our study found almost no effect of $scCO_2$ processing at 100 °C on the conductivity of the P3 sample. This implies that the highly crystalline complex domains prevented the permeation of CO_2 molecules.

It is important to discuss the relation between the ionic conductivity and the added salt concentration,

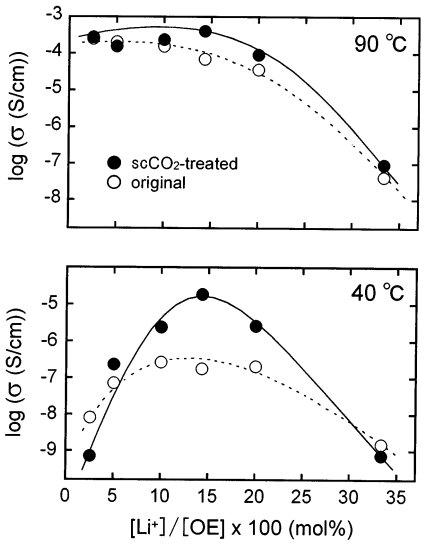

Figure 4. Variation of ionic conductivity at 40 and 90 °C vs the Li^+ to oxyethylene (OE) unit concentration ratio for the original and $scCO_2$-treated samples.

because increasing the salt concentration leads to a drastic change in phase structure, which in turn affects ionic conduction in the PEO. The change causes an increase in T_g and also a decrease in the melting point and heat of fusion, corresponding to the PEO crystal. In particular, the growth of a second T_m peak in the PEO−$LiCF_3SO_3$ system above 100 °C, related to the crystalline complex domains, is observed with increasing salt concentration. From the phase diagram studied by Prud'homme et al., a clear liquidus curve is obtained below the P3 sample, and a discontinuity occurs near the P2 sample.[31] Figure 4 summarizes the relation between the ionic conductivity at 40 and 90 °C and the Li cation concentration for the original and $scCO_2$-treated samples. The conductivity at 40 °C for the original sample showed a maximum at approximately 10 mol % Li^+ concentration. This behavior of the PEO−$LiCF_3SO_3$ system is well-known as reported by Robitaille and Fauteux.[29] At high salt concentrations above 10 mol %, the conductivity slowly decreases with increasing Li^+ concentration at both temperatures. This is due to the increase in cross-linking structures formed between PEO chains and ions, which prevents the segmental motion of local PEO chains in the amorphous regions and gives rise to the large increase in T_g. By contrast, the $scCO_2$-treated samples showed different conduction behavior. The lowest Li^+ concentration sample, P40, underwent a 10-fold decrease in ionic conductivity at 40 °C with $scCO_2$ processing, since many crystal PEO domains still remained. However, a large increase in the conductivity was clearly observed in $scCO_2$-treated samples in the middle of the Li^+ concentration range. Moreover, the maximum value shifted slightly to the higher Li^+ concentration region, from 10 to approximately 14 mol % at 40 °C. This is an important consequence of $scCO_2$ processing, which is related to salt dissociation in PEO. These results suggest that CO_2 molecules permeated into a PEO−salt mixture act as an initiator for dissociating the aggregated ions which prohibit the migration of free ions. Jun et al. have investigated the difference in ionic conductivity of lithium acetate ($LiCH_3CO_2$) and lithium perfluoroacetate ($LiCF_3CO_2$) under sub- and supercritical conditions with a small amount of methanol as an entrainer.[27] They found that the conductivity of $LiCF_3CO_2$ increases dramati-

Table 1. Glass Transition Temperature (T_g), Melting Point (T_m), and Heat of Fusion (ΔH) of PEO−$LiCF_3SO_3$ Original and $ScCO_2$-Treated Samples from DSC Measurement

	T_g (°C)		T_{m1} (°C)		T_{m2} (°C)		ΔH_1 (kJ/mol)		ΔH_2 (kJ/mol)	
sample	original	$scCO_2$	original	$scCO_2$	original	$scCO_2$	original	$scCO_2$	original	$scCO_2$
PEO	−66	−66	66	66			7.0	7.0		
P40	−54	−54	63	61			6.2	6.2		
P20	−55	−60	62	59			5.3	5.3		
P10	−55	−56	59	58	142	143	3.0	3.0	0.8	0.7
P7	−52	−58	62	59	152	153	2.5	2.2	1.6	1.3
P5	−53	−55	60	57	168	167	1.5	1.5	2.5	2.3
P3					180	180			4.0	4.1

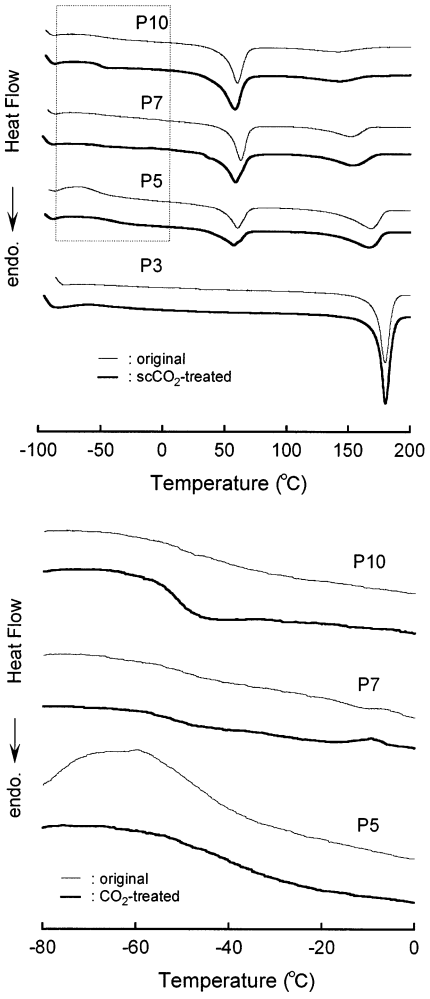

Figure 5. DSC curves for (top) P10, P7, P5, and P3 of the original and $scCO_2$-treated samples on a whole scale and for (bottom) the P10, P7, and P5 samples on an expanded scale at the glass transition region.

cally with increasing CO_2 pressure, whereas that of $LiCH_3CO_2$ decreases. They suggest that this is due not only to the salt solubility for CO_2 but also to the quadrupole−dipole interaction between CO_2 and the CF_3 group, which makes the salt more CO_2-philic and therefore increases dissociation. In the PEO−salt mixture system, therefore, the increase in ionic conductivity is caused by the dissociation effect of CO_2 on ionic aggregates such as triple ions, which increases T_g.

Thermal Analysis. Figure 5 shows the various DSC curves for the original and $scCO_2$-treated samples with added salt concentration varying from 10 to 33.3 mol %. Each original sample had a T_g of approximately −50 °C; this is a very weak transition because of coexistence in the crystalline domains of crystal PEO and the complex. In contrast, the glass transition of the $scCO_2$-treated samples, particularly the P10 sample, was clearly confirmed. This indicates that the amorphous regions in which carrier ions can migrate faster increase through the $scCO_2$ processing. A first endothermic peak was observed at approximately 60 °C, T_{m1}, corresponding to the melting of crystal PEO, in all original samples except for P3. A broad endothermic peak, which is attributed to the disordered nature of the crystal PEO domains, was observed in $scCO_2$-treated samples of P7 and P5. The reduction in T_{m1} of the original samples was caused by $scCO_2$ processing, and is related to the decrease in the crystallite size of PEO. It seems that the heat of fusion ΔH_1, which is in proportion to crystallinity, decreases as the added salt concentration increases as a result of the increase of local structure caused by the ion−dipole interactions between the Li cation and the oxygens of polyether chains in amorphous regions, which inhibits the crystallization. A second endothermic peak, T_{m2}, corresponding to the presence of crystalline complex domains, was confirmed above 120 °C. Both T_{m2} and the peak fraction ΔH_2 increase as the added salt concentration increases. According to the phase diagram,[29] a weak T_{m2} peak in the intermediate salt concentration samples such as P10 and P7 indicates very small amounts of the crystalline complex domain. However, there are almost no differences in T_{m2} and ΔH_2 between the original and $scCO_2$-treated samples.

Table 1 summarizes the DSC data of all samples. As the added salt concentration increases, a small increase in T_g is observed for both the original and $scCO_2$-treated samples. Moreover, we are able to identify clear decreases of T_{m1} and ΔH_1 related to the diminishing crystal PEO domains, and increases of T_{m2} and ΔH_2 related to the development of crystalline complex domains. Previous studies[8−10] explain that the changes with increasing salt concentration are due to increased cross-linking structures in amorphous regions, on the basis of the interaction between cations or aggregated ions and ether oxygens of the PEO chain. Here, we have confirmed that there are three main effects of $scCO_2$ processing on the thermal properties of the PEO−$LiCF_3SO_3$ system. First, a decrease in T_g is observed in four samples, from P20 to P5, whereas there is no change in T_g for pure PEO and the P40 sample. The processing enhances polyether chain mobility in the amorphous region and improves the conductivity. It inhibits the large increase of T_g caused by the increasing salt concentration, which is related to the formation of cross-linking structures between cations and polyether oxygens. The second effect of $scCO_2$ processing is the reduction in T_{m1} corresponding to melting of crystal PEO. The T_{m1} of all original samples was probably reduced, since the crystallite size of the PEO domains decreases with $scCO_2$ processing. In contrast, there was almost no differences in T_{m2} between the original and $scCO_2$-treated samples. The third effect of the processing

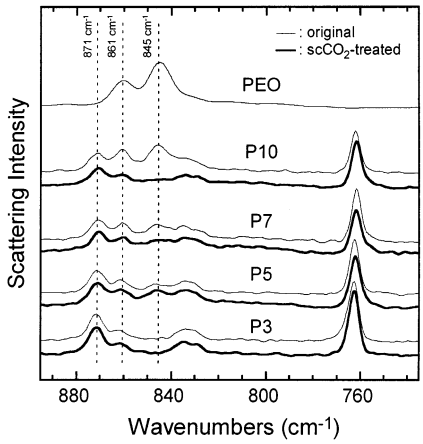

Figure 6. Raman spectra of the original and $scCO_2$-treated samples and pure PEO in the region 750−890 cm^{-1}.

is a small reduction in ΔH_2, corresponding to the melting enthalpy of crystalline complex domains (except for the P3 sample), although no difference in ΔH_1 between the original and $scCO_2$-treated samples is observed. This implies that the small decrease in ΔH_2 is related to the reduction of the relative quantity of the complex domains. On the basis of these observations, we expect that the improvement of ionic conductivity seen in Figure 4 is caused by the dissociation effect of $scCO_2$ processing on aggregate ions with high bonding energy, which gives rise to the decrease of T_g, T_{m1}, and ΔH_2. In the case of only the P7 system, it is thought that the treated sample showed more than 100-fold increase in the conductivity because of a slight reduction in the ΔH_1 in addition to the overall decreases.

Raman Scattering Study. Vibrational spectroscopic analysis has been used to characterize the conformational changes of polymers and the disposition of associated ions in polyether electrolytes. Torell et al. studied ion pairing effects in amorphous poly(propylene oxide)−salt mixture systems.[32,33] They concluded[33] that the major effect governing the enhancement of ionic conductivity at low salt concentrations is an increase in the number of dissociated ions, and that the mobility was less important in this concentration range; the conductivity drop at high concentration is due to reduced ionic mobility. It follows that an important factor in giving high conductivity is inhibition of the increase of T_g. We believe that the increase in T_g, related to the reduction of polymer chain mobility, is mainly a result of increasing the number of associated ions, which is related to the increase in local viscosity. Particularly in the case of the PEO system, crystalline complex domains consist of anions, and coordinated cations with PEO chains are produced when large amounts of alkali-metal salts such as $LiCF_3SO_3$, $NaClO_4$, and NaI are added. Recently, Frech et al. have indicated that free ions, ion pairs, triple ions, and complex domains in high molecular weight PEO can be identified using FT-IR[34−37] or Raman scattering analysis.[37,38] Following these reports, we study the effect of $scCO_2$ processing on ionic conditions in PEO using these techniques.

Figure 6 compares Raman spectra of the original and $scCO_2$-treated samples for P10, P7, P5, and P3 and pure PEO. Peaks in pure PEO at 845 and 861 cm^{-1} are identified as contributions from the crystalline fraction, corresponding to mixed CO stretching and CH_2 rocking modes. As the added salt concentration in PEO increases, the scattering intensity of these peaks decreases. In all PEO−salt mixture samples the broad peaks in this frequency range were identified as disordered nature peaks, from mixed crystalline pure PEO and complex domains. After $scCO_2$ processing, the decrease of the peak at 845 cm^{-1} in P7 and its disappearance in P10 were confirmed. In contrast, the peak at 871 cm^{-1} and the broad feature around 830 cm^{-1} corresponding to the crystalline complex domains increase with increasing salt concentration. Almost no change in peak intensity is detected between the original and $scCO_2$-treated samples. A peak at approximately 760 cm^{-1} is identified as the C−F symmetric deformation mode, $\delta_s(CF_3)$, corresponding to the CF_3 group in triflate anions. We confirm that the peak intensity of $\delta_s(CF_3)$ increases slowly with increasing salt concentration.

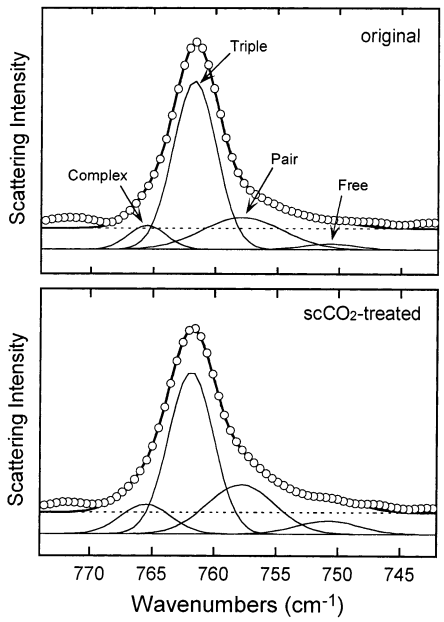

Figure 7. Raman spectra of P7 original and $scCO_2$-treated samples in the symmetric deformation region, $\delta_s(CF_3)$, with curve-fitting analysis.

Raman spectra of the original and $scCO_2$-treated samples of P7 in the region from 740 to 770 cm^{-1} are shown in Figure 7. The $\delta_s(CF_3)$ peak can be resolved into a minor "free ion" component at 752 cm^{-1}, a contribution from a contact "ion pair" at 757 cm^{-1}, a dominant band "triple ion" at 762 cm^{-1} originating in the $[Li-CF_3SO_3-Li]^+$ entity, and a crystalline "complex" at 766 cm^{-1}.[38] These are illustrated in Figure 8. The frequency of the complex component band was higher than that of the triple ions. This is attributed to the crystal packing effect of complex domains as a result of the interaction between polyether chains with Li cations and coordinated anions. The local potential energy environment of triflate anions in the triple ions differs from that in the crystalline complex.[38] After $scCO_2$ processing, a small decrease in the triple ion component of the peaks, and increases in the free ion, ion pair, and crystalline complex components were detected in Figure 7.

Table 2 summarizes the proportions of these species of high Li salt concentration samples. As the Li salt concentration increases, an increase of the complex fraction at 766 cm^{-1} and a reduction of the ion pair fraction at 757 cm^{-1} were clearly observed in both the original and $scCO_2$-treated samples. However, there were no obvious changes in the triple ion fraction at 762

Table 2. Peak Fraction of the Triflate Anion from Curve-Fitting Analysis of Raman Spectra of the $\delta_s(CF_3)$ Region[a] and Ionic Conductivity at 40 °C

	complex (766 cm^{-1})		triple ion (762 cm^{-1})		ion pair (757 cm^{-1})		free ion (752 cm^{-1})		σ (S/cm) at 40 °C	
sample	original	$scCO_2$	original	$scCO_2$	original	$scCO_2$	original	$scCO_2$	original	$scCO_2$
P10	12	5	58	53	24	40	6	2	2.7×10^{-7}	2.4×10^{-6}
P7	8	11	66	56	23	26	3	7	1.8×10^{-7}	1.8×10^{-5}
P5	23	30	65	53	4	13	8	4	2.1×10^{-7}	2.6×10^{-6}
P3	42	44	56	52	2	4	0	0	1.5×10^{-9}	7.4×10^{-10}

[a] The error in calculating each percent area is estimated to be less than ±0.5%.

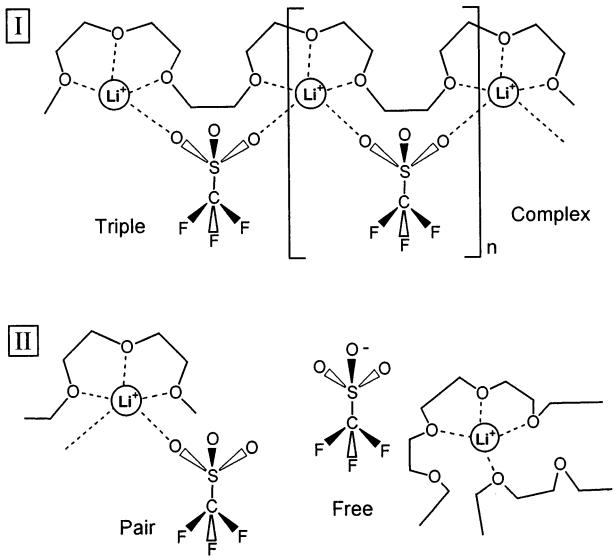

Figure 8. Schematic structures of ions in (I) the crystalline complex domain and (II) amorphous PEO.

cm^{-1} and the free ion fraction at 752 cm^{-1}, which directly contribute to the ionic conductivity. The decrease of conductivity with increasing salt concentration is mainly due to the growth of crystalline complex domains where the fast migration of ions is restricted. A decrease of the triple ion fraction and an increase of the ion pair fraction were clearly confirmed following $scCO_2$ processing for each sample. In the P10, P7, and P5 samples in particular, these variations are related to improvement of polyether chain mobility in amorphous regions, which reduces T_g (see Table 1) and increases the ionic conductivities. These results indicate that CO_2 molecules permeated into the samples under supercritical conditions mostly influence the amorphous region, in which carrier ions can migrate faster. There are no large differences between the original and $scCO_2$-treated samples in the percentages of ion fractions and the conductivity of the P3 sample, which contains a great amount of crystalline complex domains. The P7 sample showed a more than 100-fold improvement in conductivity, since the CO_2 effectively acted on the disordered nature and increased the free ion fraction. Here, we propose that the components of the complex and triple ion fractions in the high-frequency regions and the ion pair and free ion fractions at low frequencies should be classified, respectively, as immobile (type I) and mobile (type II) ion species. The "monodentate" ion pair component classified as a mobile species (type II) can increase the conductivity, since the anions are energetically similar to free ions.[39] On the other hand, the "bidentate" triple ion component (type I) is energetically stable compared with the ion pair,[39] which strongly influences the increase in T_g. The crystalline complex component, classified as the most stable structure in this system, increases with increasing repeat unit

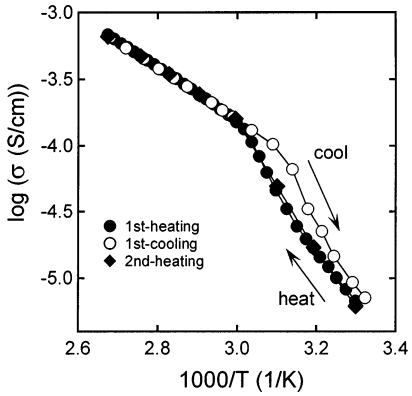

Figure 9. Temperature dependence of ionic conductivity for the P7 sample in the heating and cooling processes.

number n (Figure 8). When n is large, both the triple ions and ion pairs are identified as the terminal component of localized complex domains.[38] Conversely, when n is small, the ionic structure is governed by small aggregate ions with ion pairs. Table 2 confirms that the decrease in the triple ion fraction (totally type I) and the increase in the ion pair fraction (totally type II) are clearly caused by the $scCO_2$ processing. The result is a reduction of T_g and an increase in ionic conductivity. The processing affected the local structure consisting of these ions and reduced immobile ions such as the triple ions. Under supercritical conditions, CO_2 molecules permeated into the sample should be able to interact with Lewis bases such as triflate anions or polyether oxygens. We firmly believe that CO_2 permeation based on Lewis acid−base nature can dissociate aggregate ions, such as the triple ions, mainly in amorphous regions.

Stability of Ionic Conductivity. Figure 9 shows the temperature dependence of the ionic conductivity for the $scCO_2$-treated sample of P7 during the first heating, cooling, and second heating processes. The small gap in the conductivity plots between the first heating and cooling processes below 60 °C is attributed to the delay in recrystallization of PEO. The apparent T_m in the first process shifted to a lower temperature range, from approximately 60 to 50 °C. However, there was no difference in the behavior of the ionic conductivity between the first and second heating process samples. The improvement in the conductivity caused by $scCO_2$ processing is probably permanent, and the increase is almost wholly maintained despite variation of the external environment.

We next looked at the long-term stability of the conductivity for $scCO_2$-treated samples compared with the original. Figure 10 shows the elapsed time dependence of the conductivity at 40 °C for P7 samples. The original sample showed an approximately 10-fold reduction in conductivity within 5 days, due to progressive PEO recrystallization toward an equilibrium condi-

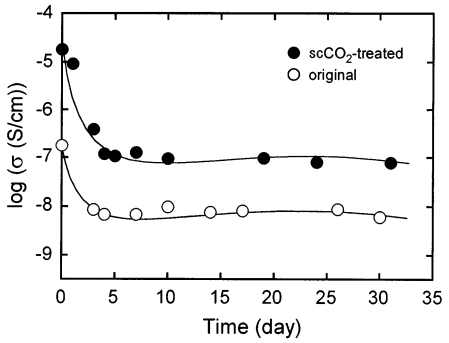

Figure 10. Ionic conductivity at 40 °C vs elapsed time in dry N_2 gas for P7 original and $scCO_2$-treated samples.

tion.[40] This indicates that the ions in their solvation sites are blocked by the rigid crystallized PEO chain structure. After 5 days the conductivity decreased gradually, with no steady value attained within the measurement period. The $scCO_2$-treated sample shows an approximately 100-fold reduction in conductivity within 5 days. In this system, inhibition of recrystallization, as seen in composite electrolytes containing γ-$LiAlO_2$, SiO_2, and TiO_2,[40,41] is not observed. The decrease in conductivity of $scCO_2$-treated samples, larger than that of the original, was caused by simultaneous reorganization involving both PEO and complex crystallization. This can be interpreted as a variation from quasi-equilibrium to the equilibrium condition of not more than 5 days. Nevertheless, the difference in ionic conductivity between the original and $scCO_2$-treated samples after recrystallization was a factor of 10, and was maintained for more than 20 days. It is mainly due to the destructive effect of CO_2 molecules on aggregate ions, such as triple ions or small complex domains, in the amorphous region. The CO_2 that had permeated into the sample as a result of the processing played a crucial role as a promoter of the dissociation of aggregate ions, on the basis of the Lewis acid−base nature.

Conclusion

We have improved the properties of crystalline PEO−$LiCF_3SO_3$ complexes using $scCO_2$ as processing solvent and measured the ionic conductivities of these complexes. A large difference in the conductivities was found between the original and $scCO_2$-treated samples. DSC measurement showed decreases of T_g, T_{m1}, and ΔH_2 in most $scCO_2$-treated samples. To analyze the changes of ionic association in PEO, we have separated the Raman peaks in the region from 740 to 770 cm^{-1} and characterized their fractions. In $scCO_2$-treated samples, the proportion of triple ions taken as immobile decreased and the ion pairs taken as mobile increased, compared with those of the original samples. The subsequent time dependence of the conductivity in the $scCO_2$-treated P7 sample showed that the processed samples maintain an approximately 10-fold higher conductivity than the original ones for at least one month. We conclude that CO_2 molecules permeated into the sample play a crucial role as promoters for the dissociation of ions to improve the conductivity, according to the Lewis acid−base nature. We propose to extend our studies to realize fast ion transport in other polyether-based electrolyte systems.

Acknowledgment. Y.T. acknowledges Eno Science Foundation for a young scientist's grant-in-aid. This work was partially supported by The 21st Century COE program from the Ministry of Education, Culture, Sports, Science, and Technology.

References and Notes

(1) Wright, P. V. *Br. Polym. J.* **1975**, *7*, 319−327.
(2) Armand, M. B.; Chabagno, J. M.; Duclot, M. T. In *Fast Ion Transport in Solids*; Vashishta, P., Mundy, J. N., Shennoy, G. K., Eds.; Elsevier: Amsterdam, 1979; p 131.
(3) Tarascon, J.-M.; Armand, M. *Nature* **2001**, *414*, 359−367.
(4) Nogueira, A. F.; Durrant, J. R.; De Paoli, M. A. *Adv. Mater.* **2001**, *13*, 826−830.
(5) Kreuer, K.-D. *Chem. Mater.* **1996**, *8*, 610−641.
(6) Miyatake, K.; Fukushima, K.; Takeoka, S.; Tsuchida, E. *Chem. Mater.* **1999**, *11*, 1171−1173.
(7) Takeoka, S.; Ohno, H.; Tsuchida, E. *Polym. Adv. Technol.* **1993**, *4*, 53−73.
(8) Gray, F. M. *Solid Polymer Electrolytes*; VCH: New York, 1991.
(9) Bruce, P. G. *Solid State Electrochemistry*; Cambridge University Press: Cambridge, 1995.
(10) Ratner, M. A.; Shriver, D. F. *Chem. Rev.* **1988**, *88*, 109−124.
(11) Tominaga, Y.; Izumi, Y.; Kwak, G. H.; Asai, S.; Sumita, M. *Mater. Lett.* **2002**, *57*, 777−780.
(12) Kwak, G. H.; Tominaga, Y.; Asai, S.; Sumita, M. *Electrochim. Acta* **2003**, *48*, 1991−1995.
(13) Kendall, J. L.; Canelas, D. A.; Young, J. L.; DeSimone, J. M. *Chem. Rev.* **1999**, *99*, 543−563.
(14) Cooper, A. I. *J. Mater. Chem.* **2000**, *10*, 207−234.
(15) Sun, Y.-P. *Supercritical Fluid Technology in Materials Science and Engineering*; Marcel Dekker Inc.: New York, 2002.
(16) Rindfleisch, F.; DiNoia, T. P.; McHugh, M. A. *J. Phys. Chem.* **1996**, *100*, 15581−15587.
(17) Kirby, C. F.; McHugh, M. A. *Chem. Rev.* **1999**, *99*, 565−602.
(18) Shieh, Y.-T.; Su, J.-H.; Manivannan, G.; Lee, P. H. C.; Sawan, S. P.; Spall, W. D. *J. Appl. Polym. Sci.* **1996**, *59*, 695−705.
(19) Shieh, Y.-T.; Su, J.-H.; Manivannan, G.; Lee, P. H. C.; Sawan, S. P.; Spall, W. D. *J. Appl. Polym. Sci.* **1996**, *59*, 707−717.
(20) Handa, Y. P.; Zhang, Z. *Macromolecules* **1997**, *30*, 8505−8507.
(21) Zhang, Z.; Handa, Y. P. *J. Polym. Sci., Part B: Polym. Phys.* **1998**, *36*, 977−982.
(22) Chiou, J. S.; Barlow, J. W.; Paul, D. R. *J. Appl. Polym. Sci.* **1985**, *30*, 2633−2642.
(23) Condo, P. D.; Paul, D. R.; Johnston, K. P. *Macromolecules* **1994**, *27*, 365−371.
(24) Kazarian, S. G.; Vincent, M. F.; Bright, F. V.; Liotta, C. L.; Eckert, C. A. *J. Am. Chem. Soc.* **1996**, *118*, 1729−1736.
(25) Flichy, N. M. B.; Kazarian, S. G.; Lawrence, C. J.; Briscoe, B. J. *J. Phys. Chem. B* **2002**, *106*, 754−759.
(26) Drohmann, C.; Beckman, E. J. *J. Supercrit. Fluids* **2002**, *22*, 103−110.
(27) Jun, J.; Fedkiw, P. S. *J. Electroanal. Chem.* **2001**, *515*, 113−122.
(28) Dardin, A.; DeSimone, M. J.; Samulski, E. T. *J. Phys. Chem. B* **1998**, *102*, 1775−1780.
(29) Robitaille, C. D.; Fauteux, D. *J. Electrochem. Soc.* **1986**, *133*, 315−325.
(30) Lightfoot, P.; Mehta, M. A.; Bruce, P. G. *Science* **1993**, *262*, 883−885.
(31) Vallee, A.; Besner, S.; Prud'homme, J. *Electrochim. Acta* **1992**, *37*, 1579−1583.
(32) Kakihana, M.; Schantz, S.; Torell, L. M. *J. Chem. Phys.* **1990**, *92*, 6271−6277.
(33) Schantz, S. *J. Chem. Phys.* **1991**, *94*, 6296−6306.
(34) Dissanayake, M. A. K. L.; Frech, R. *Macromolecules* **1995**, *28*, 5312−5319.
(35) Frech, R.; Chintapalli, S.; Bruce, P. G.; Vincent, C. A. *Macromolecules* **1999**, *32*, 808−813.
(36) Seneviratne, V.; Furneaux, J. E.; Frech, R. *Macromolecules* **2002**, *35*, 6392−6396.
(37) Frech, R.; Huang, W. *Macromolecules* **1995**, *28*, 1246−1251.
(38) Rhodes, C. P.; Frech, R. *Macromolecules* **2001**, *34*, 2660−2666.
(39) Huang, W.; Frech, R.; Wheeler, R. A. *J. Phys. Chem.* **1994**, *98*, 100−110.
(40) Croce, F.; Scrosati, B. *Chem. Mater.* **1992**, *4*, 1134−1136.
(41) Scrosati, B.; Croce, F.; Persi, L. *J. Electrochem. Soc.* **2000**, *147*, 1718−1721.

MA030207N